Evolution and comparative analysis of group armor- and aeroballistics of ancient and modern ruled and poly-wedge arrows*

Yu.A. Vedernikov, V.A. Levin, Yu.S. Khudyakov

Abstract. A comparative analysis of the group aero- and armor ballistics of the ancient and modern poly-wedge arrows is made. The idea formulated is to use these arrows as components of warheads of the carrier rockets for the anti-asteroid defence of the Earth and the orbital stations.

1. Evolution of ruled and poly-wedge arrows of the asian nomads at ancient times and in the middle ages

Penetrators intended for piercing the obstacles of increased strength [1], including asteroids [2], are widely used in modern technology.

A need in making similar devices has already arisen at very ancient times in the process of development of metallurgy and metal processing as well as in appearance of special protective means. The first experience gained in the development and application of penetrators intended for the perforation of non-metal protective means refers to the bronze age [3]. More efficient and perfect iron and steel penetration means of a remote action were developed in the process of mastering the iron-producing technology in the first millennium B.C.

The present paper deals with a complex of iron arrows as an object characterizing the evolution of the penetration means of a remote action in the historical past, which were manufactured and used by the Asian nomads at the ancient times and the Middle Ages, because these materials have been investigated and systematized until now in most detail [4].

Among the numerous nomad ethnoses inhabiting the Euro-Asian steppes in the 1st millennium B.C., the manufacturing and use of iron arrows was mastered by the Huns, which gave birth to the first powerful military dominion known in the Central Asia history. In the military art of the Huns, the distance battle weapons, bows and arrows, carried out the most important function—the enemy defeat at the arrow flight distance. During war battles, the Hun warriors performed massive shootings of enemy troops aiming at bringing the most possible damage to the troops and resolving the battle in their favor.

The invention of a composite, reflecting bow exceeding the performance of the bows of the preceding Scythian time in terms of the power and the range by a factor of one and half. The Hun bows possessed a much larger span and had zones of strength and elasticity fixed by bony superpositions. An increase in the range of a manual throwing weapon enabled the enemy to defeat at a distance, thus ensuring the safety of own military troops. An increased range of bows contributed to the improvement of arrow shapes to ensure their flight velocity needed, hit accuracy, and the efficiency of penetration into the surface to be defeated.

To meet the above requirements, the new shapes of poly-wedge arrowheads were developed, which proved to be new at that historical period. They were manufactured on the basis of the iron-making technology. Both the poly-wedge penetrators with a three-blade section and the ruled penetrators with a three-facet, a four-facet, and a flat section were presented within the Hun complex of iron arrowheads.

The arrowheads of an asymmetric rhombus shape with a blunt nose and slanted shoulders as well as the stratum arrows with a forwarding isolated hit element and wide blades, in which there were through rounded orifices, were the main shapes of the Hun three-blade penetrators. Such arrows were often supplied with bony balls-whistles, which produced a sharp whistling during their flight. Such arrows were oriented towards their rotation in flight and their maximum flight range and hit accuracy. The stratum arrows were intended for ensuring the depth of penetration into the surface to be defeated combined with a wide defeat area [1].

Among the penetrators, there were arrowheads with an elongated triangular and elongated rhombus shape of feathering, which possessed a midsection with a sharp angle of attack and were oriented towards surmounting a distance from the shooting target with an increased velocity. Such arrows, however, did not gain a widespread acceptance among the Huns. They can be considered to be experimental and search shapes intended for a search for optimal feathering shapes.

At the Hun times, specialized iron armor-piercing penetrators with three-facet and four-facet mid-sections and the elongated triangular shape appeared for the first time, which were intended for the perforation of the cuirass armor of the iron scaly breast accoutrements [4].

Relying on their military and technological advantage over their main enemies in the nomad world in the defeat means at long distances the Huns defeated all their enemies and established their political and military domination in the Central Asia.

Their main enemies, the ancient Mongolian tribes — syanbi, were, however, able to successfully oppose the Huns in the battle field. The syanbi warriors had a smaller defeat range of the distance battle, but possessed a more efficient weapon for a close battle and protective means. The bows of

the syanbi nomads were distinguished by a smaller span of shoulders and were able to defeat targets at close distances. The iron arrowheads with a flat and two-blade section were predominant in a set of arrows of the syanbi warriors. They had a higher flight velocity. When shooting at short distances, the velocity factor played a crucial role. To protect their warriors from shooting at far distances they put on composite helms and cuirasses owing to which they had a possibility of surmounting the distance separating them from the enemy troops and to initiate a close and hand-to-hand fighting with them [5]. The troops of heavily armored cuirass cavalry troops were intended for defeating the enemy in a close battle, who appeared within the synabi troops.

During the early Middle Ages, political and military domination in the nomad world was conquered by the ancient Turks. The Turkic warriors possessed various means for a distant battle. They had various shapes of complex composite bows. Unlike the preceding times, the Turkic bows had smaller dimensions. They were oriented towards a fast shooting into the target from a close distance. The ancient Turks had a much larger number of types of poly-wedge arrows with a three-blade section. The pentagonal and the hexagonal feathering shaped arrowheads were most popular. These arrows may be considered to prevail among the poly-wedge penetrators. Among the poly-wedge arrows there were four-blade arrowheads, which were likely to be the search shapes created for increasing the hit accuracy. The number of types of ruled penetrators had increased considerably as compared to the preceding time. The armor-piercing three-facet and four-facet arrowheads took the leading positions among them. The other arrows with arrowheads of the three-blade and the rounded section were used very rarely. The Turkic warriors probably aimed at increasing the efficiency of shooting at their enemies protected by the iron cuirasses and ring-armors for which they created the arrowheads intended for piercing the metal cuirass plates, cutting or separation of the rings of ring-armors, also, the Turkic riders had in their armament the arrows with flat arrowheads. They were used to shoot at a lightly armed enemy [4]. The most combative troops of the ancient Turkic forces consisted of the cuirass riders, who could successfully oppose shooting and attack their enemies in a close battle.

In the late 1st millennium A.D. the nomads' set of the means for a distant defeat considerably increased. In the IX–X-th centuries A.D., at the period of the military and political dominance of Kirghizes in the Central Asia, the typological variety of non-armor-piercing and armor-piercing arrows considerably increased. The given period is characterized by an intensified development of the penetration means. The number of non-armor-piercing shapes increased by the factor 12, and the armor-piercing arsenal increased by 25 types [1]. An intense search for the new shapes of poly-wedge and ruled penetrators, which would be more perfect in the functional, the aero-

dynamic, and the armor-ballistic respect, was dictated by spreading the efficient iron accoutrements and broadening the tactic possibilities of heavily armed cuirass cavalry. At the same time, the possibilities of expanding the technological development in the domain of manufacturing the weapons were supported by a developed smith artisan base, which existed in Sayan-Altai, in the Kirghiz state. An enhanced search and production expansion, first of all, of the penetrators intended for perforation of the cuirass armor corresponds to the development of the means for the individual metal protection and an increase in the heavily armored cavalry in the Kirghiz troops [3]. At that time, the universal arrows intended for a broad spectrum of use started to be used along with specialized types of arrows.

The Kirghiz warriors possessed various types of weapons for a close battle as well as efficient protection means. They were capable of operating successfully both at a distant battle phase and at approaching the enemy.

At the times of the developed Middle Ages, during the period of a political and military dominance of the Mongolian states in the Central Asia, considerable changes occurred in the military matter of nomads. They touched first of all the development of the means for conducting a distant battle. The design of the main manual throwing weapon of Mongolian nomads — the bow — undergone significant changes. The Mongolian bows had practically no bony superpositions fixing the stiffness zones. Only the frontal superpositions were retained, which were capable of strengthening the reflecting capabilities. The bow dimensions reduced. The Mongolian bows were better adjusted to a speedy shooting at short distances. Among the non-armor-piercing arrows, a passage occurred from using the three-blade arrowheads to a wide use of flat arrowheads. Owing to a higher flight velocity the flat arrows proved to be more efficient in a speedy shooting at short distances. The number of types was considerably reduced, and the complex shapes of armor-piercing arrows became out of use. A new stage of the evolution of penetrators is characterized by a search for optimal technological solutions corresponding to changes that occurred in the military matter [2].

The symmetry with respect to transonic regime (M $\approx$ 1.1) of the curve of the drag coefficient C_{x_0} versus the Mach number M ensures a methodological matching of the aeroballistics of ancient (subsonic) and the present-day (supersonic) arrows. The use of the Newton's shock theory enables the optimization of the arrowheads geometry to be conducted both for M $\approx$ 0.1 and M $\approx$ 4. In this connection, a combined classification of the ancient and present-day penetrators, using the pattern recognition theory, is allowed [6]. For the machine grouping of arrows, Tables 1 and 2 were analyzed. The results of a comparative analysis of the present-day and the ancient (the right-hand side) arrows are presented in Table 3. The 6th class of armor-piercing arrows of the ancient nomads draws attention (in the absence of the present-day analogs).

Table 1. Modern penetrators

No.	cross section	Profile	χ	λ_n	$\bar{l}_0$	$\bar{r}_b$	y	class
b_1			0	2.25	1.0	0	0.29	1
b_2			50	2.25	1.0	0	0.30	1
b_3			50	2.25	1.0	0	0.36	1
b_4			50	2.25	1.0	0	0.29	1
b_5			0	2.25	1.0	0	0.27	1
b_6			0	2.55	1.0	0	0.18	1
b_7			20	2.55	1.0	0	0.185	1
b_8			50	2.55	1.0	0	0.165	1
b_9			50	2.55	1.0	0	0.170	1
b_{10}			0	2.25	1.0	0	0.175	1
b_{11}			1	2.25	1.25	0	0.20	3
b_{12}			0	2.25	1.0	0	0.17	1
b_{13}			10	2.25	1.2	0	0.18	3
b_{14}			50	2.25	0.3	0	0.16	3
b_{15}			50	2.55	0.5	0	0.14	3
b_{16}			75	2.55	0	0	0.17	2
b_{17}			79	2.55	0	0	0.165	2
b_{18}			-45	2.5	0.5	0	0.195	3
b_{19}			45	2.5	0.5	0	0.190	3
b_{20}			79	2.5	0.5	0	0.185	3
b_{21}			-45	2.5	0.5	0	0.180	3
b_{22}			45	2.5	0.5	0	0.175	3
b_{23}			79	2.5	0.5	0	0.170	3
b_{24}			-45	2.5	0.5	0	0.195	3
b_{25}			45	2.5	0.5	0	0.185	3
b_{26}			79	2.5	0.5	0	0.180	3
b_{27}			45	2.5	0.5	0	0.190	3
b_{28}			30	2.2	0.6	0	0.360	5
b_{29}			40	2.2	0.55	0	0.320	5
b_{30}			50	2.2	0.5	0	0.29	5
b_{31}			35	2.2	0.45	0	0.28	5
b_{32}			45	2.2	0.4	0	0.27	5
b_{33}			55	2.2	0.35	0	0.25	5
b_{34}			70	2.2	0.25	0	0.26	4

No.	cross section	Profile	χ	λ_n	$\bar{l}_0$	$\bar{r}_b$	y	class
b_{35}			0	2.2	0.2	∞	0.27	4
b_{36}			45	2.2	1.25	0	0.24	3
b_{37}			0	1.87	1.0	0	0.10	1
b_{38}			0	2.84	1.0	0	0.08	1
b_{39}			0	4.05	1.0	0	0.06	1
b_{40}			0	2.0	1.0	0	0.09	1
b_{41}			40	1.3	0.6	0	0.30	2
b_{42}			41	1.3	0.4	0	0.20	2
b_{43}			45	1.3	0.6	0	0.29	2
b_{44}			50	1.3	0.8	0	0.39	2
b_{45}			45	1.3	0.4	0	0.195	2
b_{46}			50	1.3	0.6	0	0.295	2
b_{47}			55	1.3	0.8	0	0.36	2
b_{48}			50	1.3	0.4	0	0.20	2
b_{49}			55	1.3	0.6	0	0.31	2
b_{50}			60	1.3	0.8	0	0.38	2
b_{51}			61	2.5	0.4	0	0.103	2
b_{52}			65	2.5	0.6	0	0.175	2
b_{53}			69	2.5	0.8	0	0.176	2
b_{54}			66	2.5	0.4	0	0.104	2
b_{55}			70	2.5	0.6	0	0.177	2
b_{56}			74	2.5	0.8	0	0.178	2
b_{57}			72	2.5	0.4	0	0.106	2
b_{58}			75	2.5	0.6	0	0.178	2
b_{59}			78	2.5	0.8	0	0.181	2
b_{60}			60	2.0	0.6	0	0.125	2
b_{61}			50	1.3	0.57	0	0.30	2
b_{62}			53	1.3	0.64	0	0.31	2
b_{63}			58	1.3	0.8	0	0.36	2
b_{64}			48	1.3	0.57	0	0.305	2
b_{65}			60	2.0	0.57	0	0.23	2
b_{66}	n=8		57	1.3	0.6	0	0.31	2
b_{67}	n=8		59	1.3	0.6	0	0.315	2
b_{68}	n=8		61	1.3	0.6	0	0.32	2

Table 2. Ancient penetrators

Group		Type	Quantity	Class
I	1		1	4
	2		2	5
	3		10	5
	4		5	1
	5		5	4
	6		4	5
	7		1	4
	8		1°	4
	9		3	1
II	10		30	6
	11		145	3
	12		62	3
	13		284	3
	14		168	3
	15		99	3
	16		9	2
	17		7	2
	18		69	6
	19		25	3
	20		1	2
	21		2	2
	22		4	2
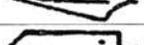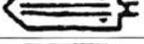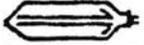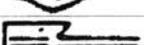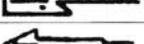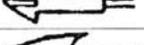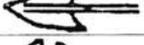
Group		Type	Quantity	Class
III	23		1	6
	24		1	4
IV	25		2	6
	26		21	6
	27		8	6
	28		26	6
	29		2	6
	30		1	6
V	31		5	6
	32		3	6
VI	33		31	6
	34		24	6
	35		8	6
	36		2	6
VII	37		42	6
	38		18	6
	39		5	6
	40		70	6
	41		16	6
	42		1	6
	43		2	6
VIII	44		10	6
	45		5	6
	46		1	2
	47		2	6
	48		6	6
	49		3	6
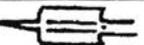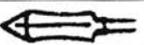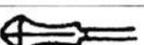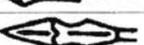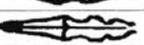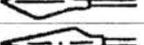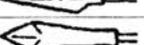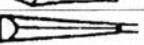
Table 3. Results of combined classification

Class	Modern penetrators	Ancien penetrators
1	41–80, 94–106, 16, 17 (star-shaped pyramidal)	1, 2, 10, 18, 23, 33, 35–37, 49, 53, 77
2	28–35, 81–93 (stepwise bodies of rotation)	
3	1, 6, 10–12, 37–39, 13–15 (complex poly-wedges)	34, 36, 46, 57, 75, 76, 78–80
4		3–9, 11–17, 19–22, 24, 54–56, 58–74 (poly-fin penetrators)
5	7–9, 18–27, 36, 40, 2–5 (simple poly-wedges)	
6		25–32, 38–41, 43–45, 47, 48, 50–52 (multisided penetrators)

In the XIII–XIV-th centuries, the Mongolian bow warriors considerably increased the efficiency of shooting at the expense of volleys. According to the information of contemporaries, the Mongolian arrows "do not fly but fall as a rain". Due to this, the defeating effect was much higher. It is not inconceivable that the Mongols had intuitively revealed the synergetic effect of the integral effect of arrows, which is much higher than the sum of separate shots. This is practically confirmed the echelon shooting, which was used by the Mongolian warriors [4].

2. The fairings formed by longitudinal translation of straight line segments and ensuring a turn around the longitudinal axis

Maikapar [7] was the first to study the aerodynamics of three-dimensional bodies with a turn around the longitudinal axis of a body. He has constructed — on the basis of the gas dynamic approach — a star-shaped body possessing a torque with respect to the longitudinal axis. Gusarov et al. [8] have also numerically determined, using the Newton approximation the configuration of a three-dimensional body with a circular mid-section, which was assembled from the ruled surfaces. In what follows we will reproduce the computation of the above-mentioned authors and present some results of wind-tunnel tests of several shapes obtained.

2.1. Mathematical design of optimal aerodynamic shapes with a torque. We will consider the ruled bodies whose initial section is formed by n segments of straight lines emanating from the same point, the mid-section being represented by a circle of radius R. Such bodies consist of n parts
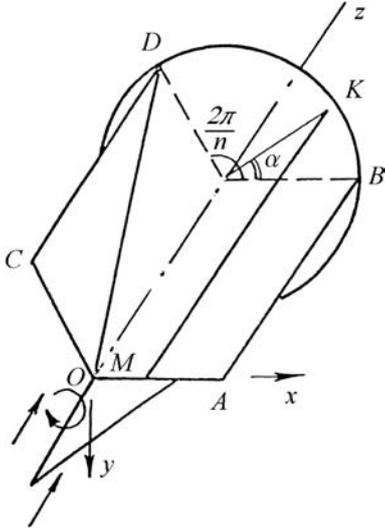
Figure 1. A ruled body

$OCDKBAO$ (Figure 1), lying in such a way that the line AB of one part is the line CD for another one. The surface $OCDKBAO$ is formed by the straight lines joining the points of the initial section with the points of the mid-section circle. A part of this surface, namely OC, is a planar triangle parallel to a free stream. Therefore, the problem will consist in determining the shape of the surface $OCDKBAO$ for which the torque with respect to the axis z will take a maximum value.

Denote the ordinate of an arbitrary point M of the initial section segment by $u \cdot R$, and the angle of the corresponding point K on the mid-section circle by α. The surface $OCDKBAO$ will then be determined by the dependence $\alpha = \alpha(u)$, and $\alpha(0) = 2\pi/n$, $\alpha(u_f) = 0$, where u_f corresponds to the point A in Figure 1. In the plane u, α the function $\alpha = \alpha(u)$ determines a curve. In order to consider the points at which $d\alpha/du$ is no longer finite, we present the dependence $\alpha = \alpha(u)$ in the parametric form $\alpha = \alpha(t)$, $u = u(t)$, where t is a parameter.

The equation of the surface $OCDKBAO$ may be written down in the parametric form [9]

$$x = \frac{R}{L}[u(t) + z(\cos \alpha(t) - u(t))], \quad y = -\frac{R}{L}z \sin \alpha(t), \quad z = z, \quad (1)$$

where z and t are parameters, and the coordinates are related to the forebody length L. The expression for the torque with respect to the axis z has the form

$$M = q \iint_S C_p(n_y x - n_x y) \, ds, \quad (2)$$

where S is the wetted surface, C_p is a pressure coefficient, ds is the elementary area, x and y are the coordinates of ds, and n_x and n_y are the projections of the normal onto ds. The normal is directed inside the surface. Taking into account the Newton law for the pressure coefficient and the surface equation (1) we rewrite expression (2) for $R/L \ll 1$ as

$$\frac{M}{q} = \frac{2nR^4}{L} \int_0^{t_f} f(u, \alpha, \dot{u}, \dot{\alpha}) \, dt, \quad (3)$$

where

$$f = \int_0^1 (1-z)(u\dot{u} + zb_1) \frac{(\dot{u} \sin \alpha - zb)^2}{az^2 - 2gz + u^2} \, dz;$$

$$a = \dot{\alpha}^2 + 2\dot{\alpha}\dot{u}\sin\alpha + \dot{u}^2, \qquad g = \dot{u}(\dot{u} + \alpha\sin\alpha);$$
$$b = \dot{u}\sin\alpha + \dot{\alpha}(1 - u\cos\alpha), \quad b_1 = \dot{u}\cos\alpha - u(\dot{u} + \dot{\alpha}\sin\alpha),$$

the dot denotes differentiation with respect to t.

We consider this integral as a function of a line parametrically specified by a representation rather than a functional depending on the two functions u and α and the parameter t. This implies that the functional should not vary when the parameter t is transformed [10]. This requirement is met in our case since it is easy to note that the function f of the four arguments u, α, $\dot{u}$, and $\dot{\alpha}$ is a positively homogeneous function of the first degree of u and α. The latter also implies that in the sequel we can assume that $\dot{u} \geq 0$. Consider the constraints, which are determined by the construction of the surfaces under study. To ensure that the surface be regular it is necessary to satisfy the condition $\dot{\alpha} \leq 0$. To eliminate the areas lying in the aerodynamic shadow we impose limitation on the length of segments of the initial section. We will assume that it does not exceed the mid-section radius, that is, $0 \leq u \leq 1$.

Let us introduce new unknown functions $\gamma(t)$ and $\beta(t)$. Then we can rewrite the inequalities $\dot{u} \geq 0$ and $\dot{\alpha} \leq 0$ in the form of the following differential equations:

$$\dot{u}(t) = \gamma^2(t), \quad \dot{\alpha}(t) = -\beta^2(t). \tag{4}$$

Therefore, the variational problem reduces to minimization of the following functional:

$$I = \int_0^{t_f} [f(u, \alpha, \dot{u}, \dot{\alpha}) + \lambda_2(t)(\dot{u} - \gamma^2) + \lambda_1(t)(\alpha + \beta^2)]\, dt,$$

where $\lambda_1(t)$ and $\lambda_2(t)$ are the Lagrange variables, or

$$I = \int_0^{t_f} F(u, \alpha, \dot{u}, \dot{\alpha}, \gamma, \beta, \lambda_1, \lambda_2)\, dt, \tag{5}$$

where $F = f + \lambda_2(\dot{u} - \gamma^2) + \lambda_1(\dot{\alpha} + \beta^2)$.

The variational problem is formulated as follows: Among the functions $u(t), \alpha(t), \gamma(t)$ and $\beta(t)$ satisfying differential equations (4) and the conditions at the ends

$$\alpha(0) = \frac{2\pi}{n}, \ \ u(0) = 0; \quad \alpha(t_f) = 0, \ \ u(t_f) = u_f, \quad u_f \leq 1, \tag{6}$$

find such functions, which maximize integral (5).

Let us write necessary conditions for the extremum:

$$F_u - \frac{d}{dt}F_{\dot{u}} = 0; \quad F_\gamma = 0; \quad F_\beta = 0. \tag{7}$$

The latter two have the form $\lambda_1\beta = 0$; $\lambda_2\gamma = 0$. Hence, the extremal consists of arcs of the three types:

1. $\dot{\alpha} = 0, \quad \lambda_2 = 0;$
2. $\dot{u} = 0, \quad \lambda_1 = 0;$ (8)
3. $\lambda_1 = 0, \quad \lambda_2 = 0.$

On the arc of the first type, the first equation of (7) is identically satisfied, and the second equation takes the following form:

$$\frac{d\lambda_1}{dt} = 0. \tag{9}$$

Hence $\lambda_1 = $ const on the arc of the first type.

On the arc of the second type, the second equation in (7) reverts into the identity, and from the first equation we have:

$$\frac{d\lambda_2}{dt} = -\frac{2}{3}u^2\dot{\alpha}\sin\alpha\cos\alpha \cdot [3\cos\alpha - 4u\cos^2\alpha + u]. \tag{10}$$

On the arc of the third type (termed the regular form) the Euler equations take the form

$$f_u - \frac{d}{dt}f_{\dot{u}} = 0; \quad f_\alpha - \frac{d}{dt}f_{\dot{\alpha}} = 0.$$

Since the extremal can contain arcs of the three types, it is natural to take into account the matching conditions at the angular points, which have the following form:

$$\Delta(F - \dot{u}F_{\dot{u}} - \dot{\alpha}F_{\dot{\alpha}}) = 0; \quad \Delta F_{\dot{u}} = 0; \quad \Delta F\dot{\alpha} = 0, \tag{11}$$

where the symbol $\Delta(\ldots)$ means the difference between the values of a specific quantity on the left and on the right from the angular point. The first of equalities (11) is identically satisfied by virtue of homogeneity of the function F with respect to $\dot{u}$ and $\dot{\alpha}$. Since the intervals of the boundary of the variation domain of u and α belong to the first and the second types of the extremal arcs, it is natural to consider necessary conditions for the extremum at the boundary [11, 12].

The intervals $\alpha = 0$ correspond to the flat winglets parallel to the flow and do not give a torque. Therefore, we eliminate them from further consideration. Let us investigate the intervals on the straight line $u = 1$. They admit the one-sided variations $\delta u \leq 0$. Therefore, the inequality

$$\left[F_u - \frac{d}{dt}F_{\dot{u}}\right]_{u=1,\ \dot{u}=0} \geq 0$$

will be a necessary condition for a maximum, which may be rewritten as

$$0 \geq \frac{d\lambda_2}{dt}\Big|_{u=1} + \frac{2}{3}\dot{\alpha}\sin\alpha\cos\alpha \cdot [3\cos\alpha - 4\cos^2\alpha + 1]. \qquad (12)$$

In addition, at the points of joining the boundary intervals $u = 1$ with arcs of the extremal, the following conditions must be satisfied:

$$\Delta F_{\dot{\alpha}} = 0; \quad \Delta F_{\dot{u}} \geq 0. \qquad (13)$$

In order to explain our choice of the signs in the above inequalities, we emphasize once again that we consider here the problem of a maximum of a functional in contrast to the conventional task of finding a minimum. The corresponding relations on the line $u = 0$ take the following form:

$$\frac{d\lambda_2}{dt} \geq 0; \quad \Delta F_{\dot{\alpha}} = 0; \quad \Delta F_{\dot{u}} \leq 0. \qquad (14)$$

The Legendre condition is a necessary condition for a maximum on the extremals:

$$F_{\dot{u}\dot{u}}(\delta\dot{u})^2 + 2F_{\dot{u}\gamma}\delta\dot{u}\,\delta\gamma + F_{\gamma\gamma}(\delta\gamma)^2 + F_{\dot{\alpha}\dot{\alpha}}(\delta\dot{\alpha})^2 + 2F_{\dot{\alpha}\beta}\delta\dot{\alpha}\,\delta\beta +$$
$$F_{\beta\beta}(\delta\beta)^2 + 2F_{\dot{u}\beta}\delta\dot{u}\,\delta\beta + 2F_{\dot{\alpha}\gamma}\delta\dot{\alpha}\,\delta\gamma + 2F_{\dot{u}\dot{\alpha}}\delta\dot{u}\,\delta\dot{\alpha} \leq 0,$$

where $\delta(\ldots)$ is a variation calculated at a constant value.

Let us express the variations $\delta\beta$ and $\delta\gamma$ from (4) in terms of $\delta\dot{u}$ and $\delta\dot{\alpha}$, then the latter inequality takes the form

$$f_{\dot{u}\dot{\alpha}}\delta\dot{u}\,\delta\dot{\alpha} + \left(f_{\dot{\alpha}\dot{\alpha}} - \frac{\lambda_1}{2\dot{\alpha}}\right)(\delta\dot{\alpha})^2 + \left(f_{\dot{\alpha}\dot{\alpha}} - \frac{\lambda_2}{2\dot{u}}\right)(\delta\dot{u})^2 \leq 0. \qquad (15)$$

Hence $\lambda_1 \leq 0$ on the arc of the first type, whereas $\lambda_2 \geq 0$ on the arc of the second type, and on the arc of the third type

$$f_{\dot{\alpha}\dot{\alpha}}(\delta\dot{\alpha})^2 + f_{\dot{u}\dot{\alpha}}\delta\dot{\alpha}\delta\dot{u} + f_{\dot{u}\dot{u}}(\delta\dot{u})^2 \leq 0. \qquad (16)$$

Since u_f is indeterminate, it is necessary to account for the transversality condition, whose general form is the following:

$$[(F - \dot{u}F_{\dot{u}} - \dot{\alpha}F_{\dot{\alpha}})\delta t + F_{\dot{u}}\delta\dot{u} + F_{\dot{\alpha}}\delta\dot{\alpha}]\big|_{u=u_f} = 0.$$

Since F is a homogeneous function of u and α, and $\alpha(t_f) = 0$, then the transversality condition takes the form

$$F_{\dot{u}}\big|_{t=t_f} = 0. \qquad (17)$$

It was found above that the extremal may consist of arcs of the three types. Considerable difficulties arise in the analytical investigation of the

arcs of the third type, which are related to the fact that the Euler equations are intrinsically nonlinear in this case and have second order. We will, therefore, construct an extremal from the arcs of the first two types. Let us show that in this case there can be no more than two corner points. Indeed, we obtain on the arc of the first type ($\alpha = \text{const}$) from the Euler equation (9) and the condition at the node points (11): $\cos^2\alpha \cdot u_1(3 + u_1^2) = \cos^2\alpha \cdot u_2(3 + u_2^2)$, where u_1 and u_2 correspond to the ends of the interval $\alpha = \text{const}$. This equality is satisfied only at $\alpha = \pi/2$. Hence for $n \geq 4$ our assertion is true. Furthermore, in this case the extremal may have only one node point (Figure 2a). The validity of the assertion for $n = 3$ and $n = 2$ follows from a similar relationship along the arc of the second type ($u = \text{const}$), whose ends are represented by the points $\alpha = \pi/2$ and $\alpha = \pi/n$. Let us integrate equation (10) over this arc:
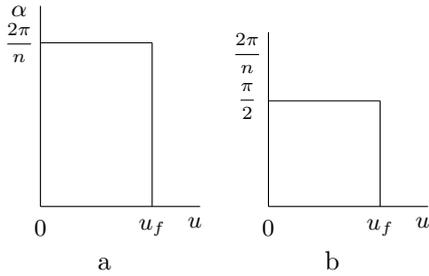
Figure 2. The domain of parameter variation in the plane (u, α) (a) and the extremals (b)

$$\lambda_2\left(u, \frac{2\pi}{n}\right) - \lambda_2\left(u, \frac{\pi}{2}\right) = \frac{2}{3}u^2\cos^2\frac{2\pi}{n}\left[\cos\frac{2\pi}{n} - \cos^2\frac{2\pi}{n}\right]. \qquad (18)$$

Substituting from (11) the expression for the second Lagrange multiplier, we obtain the equation for determining u:

$$\cos^3\frac{2\pi}{n}(1 + u^2) = 0,$$

that is, there is no arc of the second type with the ends $\alpha = 2\pi/n$ and $\alpha = \pi/2$, which would lie inside the region $0 \leq u \leq 1$, $0 \leq \alpha \leq 2\pi/n$. Consequently, for $n \leq 3$, the extremal may have no more than two corner points (Figure 2b).

From the transversality condition (17) we have:

$$\lambda_2 = -\frac{1}{3}(1 - u_f)^2(u_f + 0.5) \leq 0,$$

which contradicts the Legendre condition for all u_f except for $u_f = 1$. On the intervals $u_f = 1$, it is necessary to investigate the conditions of an extremum at the boundary. From (13) we have:

$$\lambda_1 = \frac{2}{3}\sin\frac{2\pi}{n}\cos^2\frac{2\pi}{n}\left[\cos\frac{2\pi}{n} - 1\right] \leq 0. \qquad (19)$$

$$\lambda_2 \le -\frac{2}{3}\cos^4\frac{2\pi}{n} + \cos\frac{2\pi}{n}. \tag{20}$$

The inequality $F_u|_{t=t_f} \ge 0$ will be the transversality condition, or $\lambda_2(1,0) \ge 0$. We set $\lambda_2 = 0$ at the point $u = 1$, $\alpha = 0$, which is the least value, satisfying the foregoing inequality. Then we obtain from (12):

$$\lambda_2(1,\alpha) \ge -\frac{1}{3} + \frac{2}{3}\cos^2\alpha(\cos\alpha - \cos^2\alpha + 0.5). \tag{21}$$

We obtain from (20) and (21) that the interval $u \approx 1$, $0 \le \alpha \le 2\pi/n$ will belong to the maximizing curve only for the values $n \ge 4$. Thus, for $n \ge 4$, the maximizing curve has the form shown in Figure 2a, where $u_f = 1$, and consists of the segments $u = 1$ and $\alpha = 2\pi/n$. The corresponding optimal body for $n = 4$ and its cross-section are shown in Figure 3. The expression for the torque (3) takes the following form (for $n \ge 4$):

$$M = \frac{qR^4 n}{3L}\left[\sin^2\frac{2\pi}{n}\left(1 + \cos\frac{2\pi}{n}\right) + \frac{\left(1 - \cos\frac{2\pi}{n}\right)^3}{3}\right]. \tag{22}$$

The moment reduces when a body rotates around the axis in the positive direction. It is seen from (22) that at $n \to \infty$, the torque magnitude tends to zero.

Note the fact that the surface of the ruled bodies obtained of a maximum longitudinal moment is close in its shape to the surface of the bodies with a minimum drag [8]. It is, therefore, not surprising that the drag of the bodies
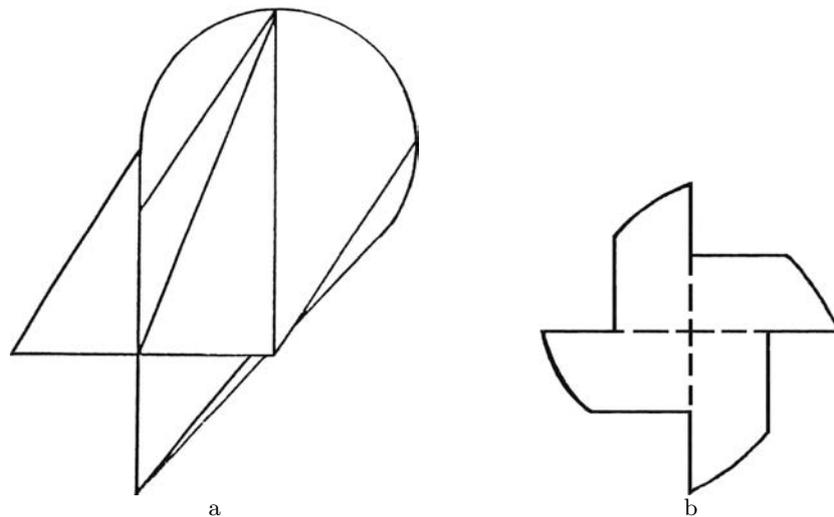

Figure 3. The optimal ruled forebody with a turn around the longitudinal axis: (a) the general view; (b) the forebody cross-section

obtained is less than that of an equivalent (in terms of the length and the mid-section radius) bodies of revolution. So, for $n = 4$, the wave drag of the body depicted in Figure 3 amounts to 72 % of the equivalent cone drag.

Note that for the bodies considered here, the force component in the direction of the longitudinal axis (the drag force) and the moment relative to this axis are different from zero, and the remaining components of the force as well as moments are equal to zero.

2.2. Description of aerodynamic models and the techniques of wind tunnel tests on a rotating sting.

The wind tunnels are subdivided into "continuous" and "periodic" types [13]. The wind tunnels of a continuous action are used in a wide range of flow speeds. The pressure tank units of a periodic action with a discharge into the atmosphere and the tunnels that operate at atmospheric pressure with a discharge into a vacuum chamber are usually used with the Mach numbers from 0.5 to 5. The tunnels that operate at a high pressure with a discharge into a vacuum tank are used with high Mach numbers. Being simple in structure, the periodic action tunnels are inferior to the continuous action tunnels in terms of the amount of experimental data. Great many instruments for static measurements are used in the continuous action wind tunnels in addition to the high-speed equipment, which is also used in the periodic action tunnels. A continuous action tunnel has a longer operating time. This makes it possible to carefully check the results of measurements and to repeat the measurements when necessary.

A compressor drives the air in a tunnel. Nozzle inserts govern the flow mode required. The test section of a tunnel, where the model under study is installed, is equipped with pressure gauges of different types, which monitor the mode of flow. The loads carried by the model are measured by an external mechanical balance or by an internal strain-gauge balance inside the model. Since the strain-gauge balance is difficult to calibrate, the mechanical balance with measurement accuracy of 1 to 2 % are widely used. The supersonic T-313 wind tunnel at the Institute of Theoretical and Applied Mechanics of the Siberian Branch of the Russian Academy of Sciences (ITAM SB RAS, Novosibirsk, Russia), where the majority of our tests on poly-wedge and axillary symmetric arrows were carried out, is equipped as described above. A general view of this wind tunnel is shown in Figure 4. High efficiency of the experimental data processing provided by the T-313 test equipment is well known.

For the balance tests, two series, with three models in each one, were chosen, which had the forebody aspect ratios $\lambda_f = 4.05$; 2.84; 1.87. The diameter of the models was 5.5 cm, the aspect ratio of the cylindrical part being equal to unity. The first series was manufactured in a strict agreement with recommendations of the foregoing subsection. In the second series, the

Figure 4. The wind tunnel T-313

curved surface of an individual wedge was manufactured in the form of a spatial translation of a straight line segment, whose one end moved uniformly along the rectilinear leading edge of the wedge, the other end moved along the arc of its cylindrical base. Such a construction of the curved surface was inspired by the solution of Gusarov et al. [14]. Both series were manufactured with four rays, with a high purity of the treatment of surfaces. The thickness of leading edges did not exceed 0.03 cm. For each aspect ratio under study, the cones with equivalent lengths and diameters were manufactured with the mid-section area $S_M = 23.7$ cm^2.

The investigation of the models was carried out for the Mach numbers M = 2.03; 4; 6 and the Reynolds numbers $\text{Re}_{1M} = 23 \cdot 10^6$, $40 \cdot 10^6$, and $60 \cdot 10^6$, respectively. The aerodynamic characteristics were determined in the range of the angles of attack α from $-4°$ to $+12°$. The error in the balance measurements did not exceed 3 % and decreased with reduction of the forebode aspect ratio.

The tests were conducted on an improved device developed by Bychkov et al. [15] for measuring the lateral forces and moments acting on the model rotating in the wind tunnel. The possibility of using this device for measuring the frontal drag, the longitudinal force, and the moment was shown in [16]. Recommendations on the base pressure measurement from [17] were refined for the models on a rotating sting in [18].

Figure 5 presents a design diagram of a setup for the investigation of the rotation influence on aerodynamic characteristics of the models. Model *1* is mounted on sting *2* and is supported by bearings *3* and *4*. The reverse electric motor of direct current *5* with a photoelectric (or electromagnetic) tachometer ensures the measurement of the number of revolutions of the
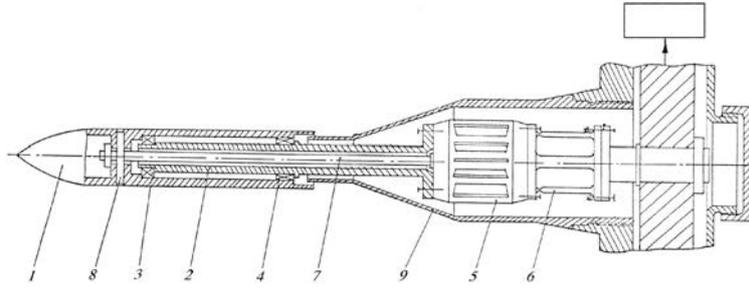
Figure 5. The design diagram of the experimental setup for
studying the rotating models

model. The isometric balance *6* enables the measurement of two components
of the total force acting on the model. The model rotation is realized by
the electric motor with the aid of the central rod *7*, which is positioned
freely inside the sting and pin *8*. When the electric motor is switched off,
self-rotation mode of the model under study is possible. Fairing *9* prevents
the setup design from the free stream effect. The entire setup is mounted
on a sabre-shaped suspension of the wind tunnel T-313. In the case of a
fixed or a self-rotating model, when the strain gauge balance is not used,
the processing of the measurement results is performed by a technique of
balance tests, which is standard for the wind tunnel T-313 [17]. The strain
gauge balance is used for measuring the Magnus forces, and the experiment
is conducted by the following technique. For a given angle of attack, two
measurements are made: with a forced or a free rotation of the model.

**2.3. Experimental refinement of aerodynamic shapes and charac-
teristics.** The first stage of experimental investigation consisted in the
choice of the most rational series of models and elucidation of their advan-
tages. Figure 6 shows the dependence of the total drag coefficient C_x for all
models versus the angle of attack α (in the absence of rotation). The curves
$C_x(\alpha)$ corresponding to the theoretically found ruled bodies are marked
with digit 1. The curves $C_x(\alpha)$ for the second series of ruled shapes are
marked with digit 2; and, finally, the curves $C_x(\alpha)$, obtained for the cone,
are marked with digit 3. It is seen that the second series of models is the
most advantageous. The model of this series with aspect ratio 2 ensures a
drag reduction by 10 % in comparison with the equivalent cone for M = 4.
Figure 7 presents, with the same digital marks for series, the dependence of
the total drag coefficient at zero incidence on the aspect ratios of the models.

The results of the tests of the first series of models for M = 3 are pre-
sented in Figure 8. It may be seen that there are practically no difference in
$C_x(\alpha)$-dependence, although the angular velocity reached the values of 30
revolutions per minute. The dependencies of the C_x coefficient on the Mach
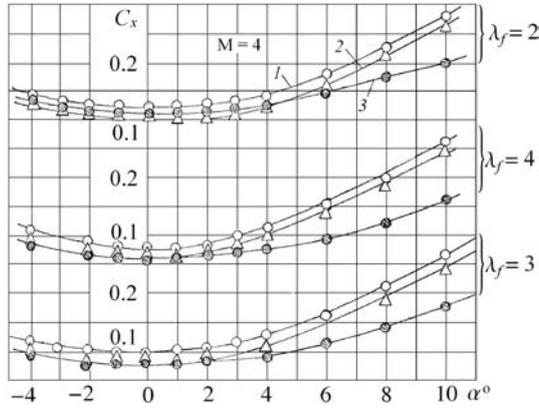
Figure 6. The dependence of the total drag coefficient C_x for all models versus the angle of attack α (in the absence of rotation)
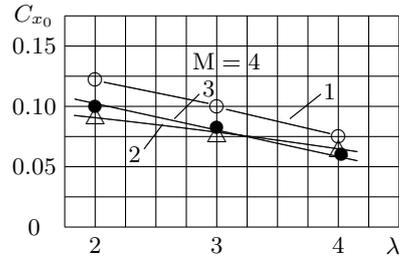
**Figure 7.** The dependence of the total drag coefficient at zero incidence on the aspect ratios of the models
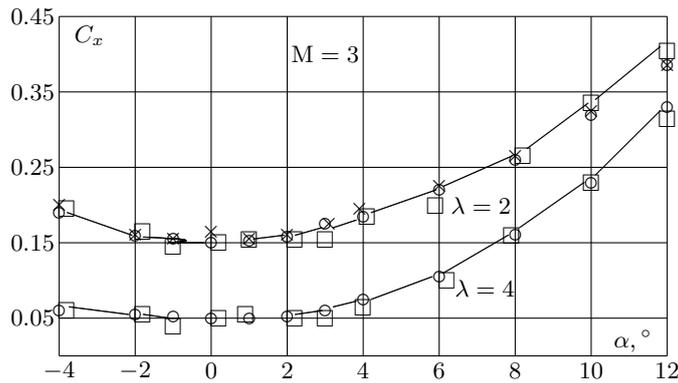
Figure 8. The total drag coefficient versus the angle of attack: ○ is the "×" poly-wedge; □ is the "+" poly-wedge; × is the rotating poly-wedge ($n = 10$–30 rev./s)

numbers for the models under study are shown in Figure 9.

The influence of the turn of ruled forebodes on the pressure center (Figure 10), the lift coefficient (Figure 11), and the longitudinal moment are also insignificant. The dependence of the pressure center abscissa $X_{\text{p.c.}}$ for small angles α for the series under investigation are presented in Figure 12. One can see that the location of the pressure center is stable for ruled forebodies, with a simultaneous increase in the gain C_{x0} with an increasing Mach number for short ruled forebodes. This stability represents an undoubted positive quality.
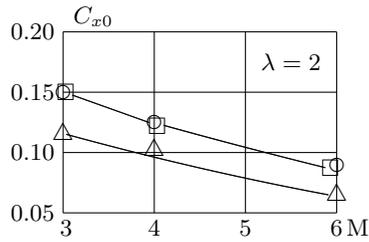
Figure 9. The total drag coefficient versus the Mach number: ∘ is the "×" poly-wedge, □ is the "+" poly-wedge; △ is the cone
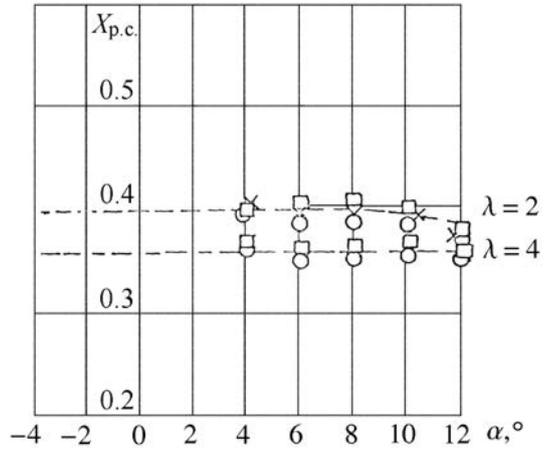
Figure 10. The pressure center location versus the angle of attack: ∘ is the "×" poly-wedge; □ is the "+" poly-wedge; × is the poly-wedge with rotation ($n = 10$–30 rev./s)
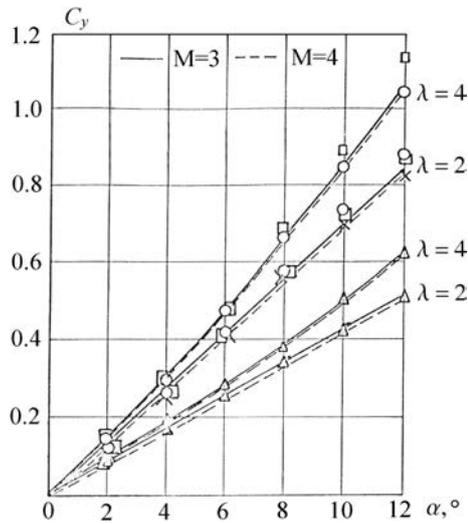
Figure 11. The lift coefficient versus the angle of attack: ∘ is the "×" poly-wedge; □ is the "+" poly-wedge; × is the poly-wedge with rotation ($n = 10$–30 rev./s); △ is the cone
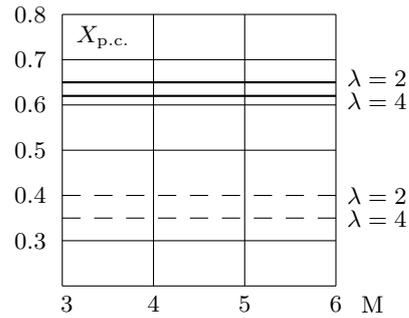

Figure 12. The pressure center abscissa versus the Mach number: — the cone; – – the poly-wedge

3. Penetration of poly-wedge and ruled bodies into metal targets

The need in investigation of armor-piercing characteristics of ruled penetrators is caused not only by the aerodynamic aspects but also by a possible improvement of anti-ricochet properties, which may be used when designing finned armor-piercing subcaliber projectiles. Tests on the perforation of metal targets by the ruled penetrators were carried out on the Russian installations specially developed for this purpose [21].

A general view of the projectiles investigated is shown in Figure 13. The projectiles are manufactured of steel 30 HGSA, and were thermally processed up to the HRC of 40, ..., 45. The armor plates of steel 2P with a thickness of 10, 14, and 16 mm, the plates of the aluminum alloy D16T with a thickness of 30 mm, and AMG-6 of 75 mm in thickness as well as a set of separated aluminum sheets of 2 mm thickness were used as obstacles.

The acceleration of penetrators was made on the powder barrel setups with a penetrator velocity variation by means of the powder amount variation. The penetrator velocity at the barrel outlet was measured with the aid of the "Neptune" chronometer. The obstacle was mounted at a distance of 2 to 5 meters from the barrel exit section. Both the penetrators and the bottom plates were carefully weighted prior the shot. The error in the velocity measurement did not exceed 2 %.

The following obstacles were used in the tests: semi-infinite and finite (moderate and thin-separated) aluminum obstacles and finite-thickness steel obstacles. At a normal penetration of a penetrator with a turn into a semi-infinite AMG-6 obstacle, a rupture of the forebode parts of nose wedges occurs, which is caused by a penetrator rotation in the process of its pen-
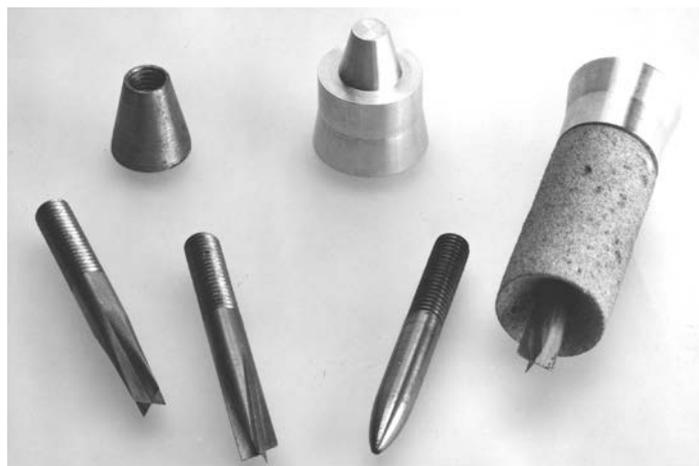
**Figure 13.** A general view of the penetrators under study
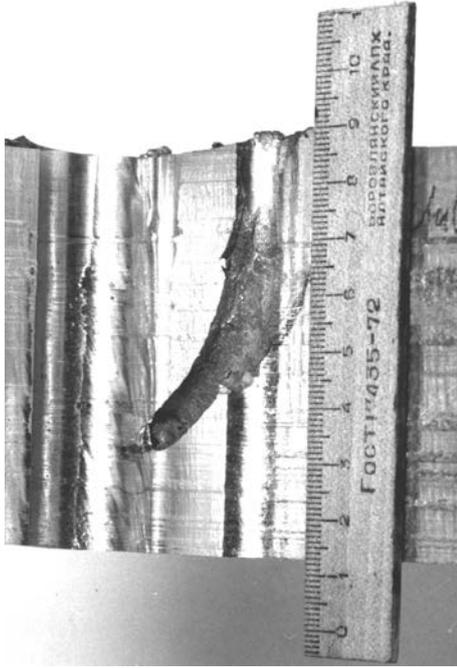
Figure 14. The curved shape of a cavity in the steel plate as a result of penetration of a projectile with ruptured nose wedges
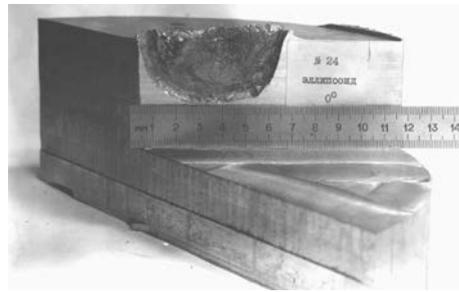
Figure 15. The cavity shape in the steel plate as a result of penetration of an axially symmetric projectile

etration into an obstacle. Figure 14 clearly shows how the penetrator with ruptured nose wedges moves. A formless configuration of this penetrator obtained in the course of penetration results in a curved motion trajectory and, as consequence, in the reduction of a penetration depth measured along a normal to the obstacle surface in comparison with the equivalent axially symmetric penetrator (Figure 15). The total length of the trajectory of the ruled penetrator may be somewhat larger than in the case of an axially symmetric penetrator. So, for the impact velocity of 1100 m/s this addition amounts to about 10 %.

When the ruled and axially symmetric projectiles penetrate along a normal into the finite obstacles of D16T (50 mm in thickness) with the velocity $V_0 = 1100$ m/s, no qualitative and quantitative difference is revealed (Figure 16).

The penetration along a normal into the steel armor of a 2P brand was carried out for a target thickness of 16 and 10 mm and impact velocities of 1100 and 700 m/s, respectively. It is seen from Figure 16 that the contours of inlets and outlets of the holes formed by a symmetric poly-wedge penetrator with a turn, and an axillary symmetric penetrator do not practically differ
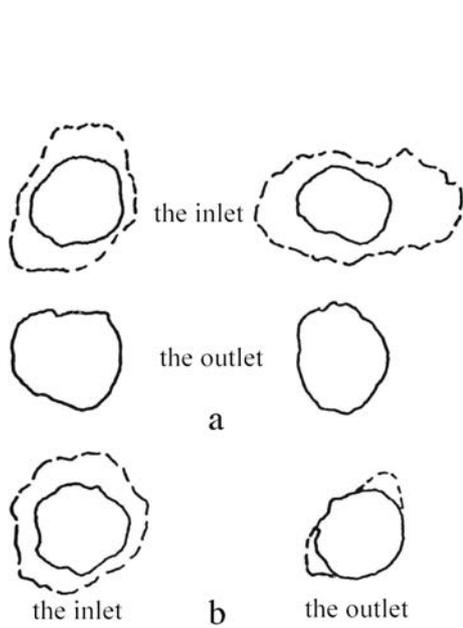
Figure 16. The contours of inlets and outlets of the holes made in the 2P armor, the obstacle thickness $\delta = 16$ mm, $V_0 = 1100$ m/s, $\alpha = 0°$: (a) the poly-wedge penetrator; (b) the equivalent axially symmetric penetrator. $--$ the spallation contour
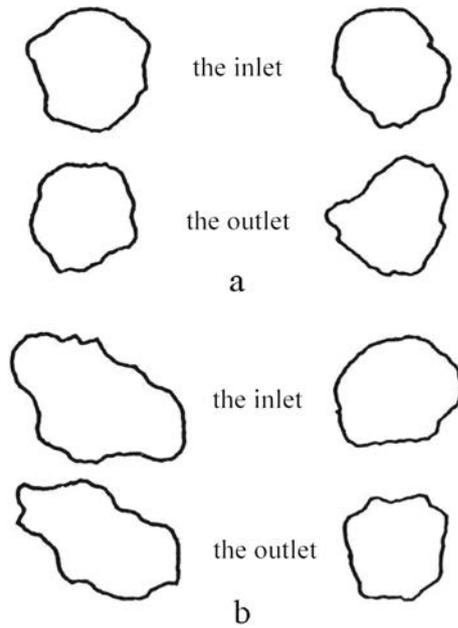
Figure 17. The contours of inlets and outlets of the holes made in the 2P armor, the obstacle thickness $\delta = 10$ mm, $V_0 = 700$ m/s, $\alpha = 0°$: (a) the poly-wedge penetrator; (b) the equivalent axillary symmetric penetrator
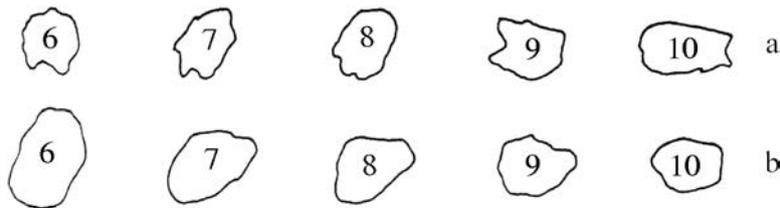
Figure 18. The contours of the holes made in the sheets of the D16T, ten sheets 2 mm in thickness, the distance between the neighboring sheets is 50 mm, $V_0 = 900$ m/s: (a) poly-wedge penetrator; (b) the equivalent axillary symmetric penetrator. The number denotes the sheet number

from one another for $V_0 = 1100$ m/s. A similar result has been obtained for $V_0 = 700$ m/s (Figure 17).

No difference has also been obtained at a normal perforation of separated obstacles representing a set of 10 duralumin sheets 2 mm in thickness with a distance of 50 mm between the neighboring sheets (Figure 18) for $V_0 =$

900 m/s. A comparative analysis of the results of penetration of penetrators at the impact angles α from $45°$ to $75°$ to the normal has revealed some difference in the penetration character.

The normal and oblique penetration of the finite steel obstacles by a compact group of symmetric ruled and poly-wedge penetrators leads for certain impact velocities to a considerable increase in the amount of the ejected material of the obstacle as compared to the equivalent axillary symmetric penetrators. The advantage of a single effect of symmetric ruled and poly-wedge penetrators is seen especially clearly for the impact with the obstacle at the angle of $30°$ to the normal, and it becomes more pronounced for the impact velocities $V_0 = 1000$–3000 m/s. The advantage of the ruled and poly-wedge penetrators become more pronounced with increasing impact velocities.

4. Conclusion

A review of the main stages of the evolution of the group aero- and armor ballistics of the ancient and the present-day arrows is presented. The aerodynamic optimization of arrow forebodies with an asymmetric cross-section has been carried out, its solutions being verified in experiment. Their comparative armor-ballistic analysis has been conducted and the anti-ricochet advantages of the ruled and poly-wedge forebodies have been identified. It is proposed to apply the ruled and poly-wedge arrows for a group effect on threatening asteroids. It is assumed here that there is a synergetic effect of a high-velocity impact of a group of arrows with a dangerous space object at an optimal distance between the impact points [21].

References

[1] Vedernikov Yu.A., Khudyakov Yu.S., Omelaev A.I. Ballistics from Arrows to Rockets. — Novosibirsk: Nauka, 1995 (In Russian).

[2] Alekseev A.S., Volkov V.A., Velichko I.I., Vedernikov Yu.A. Rocket conception of the anti-asteroid protection of the Earth // The Great Bear. — 2000. — No. 1. — P. 41–59 (In Russian).

[3] Khudyakov Yu.S. Arming of the Yenisey Kirghizes of the VI–XII Centuries. — Novosibirsk: Nauka, 1980 (In Russian).

[4] Khudyakov Yu.S. Arming of the Medieval Nomads of South Siberia and Central Asia of the VI–XII Centuries. — Novosibirsk: Nauka, 1980 (In Russian).

[5] Khudyakov Yu.S., Yui Su-Khua. The arming complex of Syanbi // Ancient Times of Altai. Digest of the Archeology Laboratory. — Gorno-Altaisk: Gorno-Altaisk State Univ., 2000. — No. 5. — P. 37–48 (In Russian).

[6] Lbov G.S. Methods of Processing of Experimental Data of Different Types. — Novosibirsk: Nauka, 1980 (In Russian).

[7] Maikapar G.I. About the shape of bodies that have drag and moment relative to the longitudinal axis in supersonic flight // Uch. zap. TsAGI. — 1976. — Vol. 4, No. 3. — P. 73–74 (In Russian).

[8] Gusarov A.A., Deyev A.A., Levin V.A. et al. Optimal aerodynamic shapes of the bodies // The IV All-Union Congress on Theoret. Appl. Mech. — Kiev: Naukova Dumka, 1976 (In Russian).

[9] Levin V.A., Vedernikov Yu.A., Gusarov A.A., Pishchulin V.S. The group aerodynamic and armor ballistics of ruled and poly-wedge bodies // The Great Bear. — 2003. — No. 1. — P. 80–86 (In Russian).

[10] Maikapar G.I. On the wave drag of non-axillary symmetric bodies in supersonic flow // Prikl. Matematika i Mekhanika. — 1959. — Vol. 23, Iss. 2. — P. 376–378 (In Russian).

[11] Lavrentiev M.A., Lyusternik L.I. Fundamentals of Variational Calculus. — Moscow: ONTI NKTN, 1935 (In Russian).

[12] Kraiko A.N. On the determination of the body of minimum drag at the use of the Newton and Busemann drag laws // Prikl. Matematika i Mekhanika. — 1963. — Vol. 27, Iss. 3 (In Russian).

[13] Klemenkov G.P., Zaleyeva V.L., Omelayev A.I. Expansion of the operation range of wind tunnel heaters // Questions of Gas Dynamics (Voprosy Gazodinamiki) / Inst. Theor. and Appl. Mech. USSR Acad. Sci. Siber. Branch. — Novosibirsk, 1975. — P. 298 (In Russian).

[14] Gusarov A.A., Dvoretskii V.M., Ivanov M.Ya., Levin V.A., Cherny G.G. Theoretical and experimental research of aerodynamic characteristics of three-dimensional bodies // Izv. AN SSSR, Mekhanika Zhidkosti i Gaza. — 1979. — No. 4. — P. 97–102 (In Russian).

[15] Bychkov N.I., Dubrovsky B.L., Kovalenko V.M., Shushpanov M.M. Device for Measuring the Lateral Forces and Moments Acting on a Model in the Wind Tunnel / USSR Authors' Certificate No. 457380 of February 18, 1972 (In Russian).

[16] Bordyug V.L., Dubrovsky B.L. The influence of rotation on aerodynamic characteristics of a rocket // Scientific and Technical Bulletin MM. — 1978. — No. 9 (In Russian).

[17] Vasenev L.G., Zuenko V.S. A computer code for processing of the results of balance tests of the models in wind tunnel T-313 on computer "Minsk-32" / Report of the Inst. Theor. Appl. Mech. ITAM USSR Acad. Sci. Siberian Branch. — 1971 (In Russian).

[18] Bordyug V.L., Vedernikov Yu.A., Dubrovsky B.L. Measurement of base pressure of artillery projectiles in wind tunnels // Scientific and Technical Bulletin MM. — 1980. — No. 1 (In Russian).

[19] Kravets V.V., Shvets A.I. About some regimes of supersonic flow around poly-wedge bodies // J. Appl. Mech. Techn. Phys. — 1974. — No. 3. — P. 59–66 (In Russian).

[20] Kravets V.V., Shvets A.I., Kazakov M.N. Aerodynamic coefficients of nonconical bodies with a star-shaped lateral cross section // Izv. AN SSSR, MZhG. — 1974. — No. 6. — P. 127–132 (In Russian).

[21] Vedernikov Yu.A., Zelepugin S.A., Kryukov B.P., Khorev I.E., Yakushev V.F. Throwing and impact of a group of high-velocity debris onto protective obstacle // The Great Bear. — 2003. — No. 1. — P. 97–106 (In Russian).